

[ Alexander M. Haimovich, Rick S. Blum, and Leonard J. Cimini, Jr. ]

# MIMO Radar with Widely Separated Antennas



© PHOTODISC

## [ Reviewing recent work ]

**M**IMO (multiple-input multiple-output) radar refers to an architecture that employs multiple, spatially distributed transmitters and receivers. While, in a general sense, MIMO radar can be viewed as a type of multistatic radar, the separate nomenclature suggests unique features that set MIMO radar apart from the multistatic radar literature and that have a close relation to MIMO communications. This article reviews some recent work on MIMO radar with widely separated antennas. Widely separated transmit/receive antennas capture the spatial diversity of the target's radar cross section (RCS). Unique features of MIMO radar are explained and illustrated by examples. It is shown that with noncoherent processing, a target's RCS spatial variations can be exploited to obtain a diversity gain for target detection and for estimation of various parameters, such as angle of arrival and Doppler. For target location, it is shown that coherent processing

*Digital Object Identifier 10.1109/MSP.2007.909532*

can provide a resolution far exceeding that supported by the radar's waveform.

## INTRODUCTION

Active arrays, applied to radar systems, have been a topic of intensive research, and are well documented in the literature from the system implementation point of view (see survey in [1]), as well as for processing techniques for target detection and parameter estimation [2]. Target parameters of interest in radar systems include target strength, location, and Doppler characteristics.

Phased-array radars with digital beamforming at the receiver have the ability to steer multiple, simultaneous beams (see, for example, [2]–[4]). Adaptive array radars process the signals received at the array elements in order to optimize some performance figure of merit, e.g., signal-to-interference ratio [5]. In airborne and other applications, the detection of moving targets and their discrimination against the background clutter are of great interest; this led to the development of array radars with space-time adaptive processing (STAP) [6], [7] (as well as recent books [8], [9]). In addition to spatial (or space-time) beamforming, signals received at an array can be processed to yield high resolution estimates of angle of arrivals of radar targets e.g., MUSIC or maximum likelihood (ML) techniques [2].

Phased-arrays with multiple transmit elements are capable of cohering and steering the transmitted energy [4]. Elements of phased-array radars are typically co-located, both at the transmitter and receiver ends. Multiple radars suitably placed may be configured to operate in multistatic mode [10]. Typically, a multistatic radar is a system that networks multiple, independent radars. Each radar performs a significant amount of local processing. Outcomes of the local processing may be delivered to a central processor through a communication link [10]. For example, individual radars of a multistatic system may perform local detection decisions, leaving the central processor the task of fusing these decisions.

In the 1990s, a new and interesting concept, employing multiple transmit elements, was introduced—synthetic impulse and aperture radar (SIAR) [11]. The SIAR transmitting array emits orthogonal waveforms. This property ensures that a receiver that processes the received mixture of signals is capable of separating and processing the waveforms individually. Through synthetic pulse formation, SIAR achieves the advantages of wideband radar (improved range resolution) but with individual antennas transmitting only narrowband waveforms. Unlike conventional beamformers, SIAR features isotropic radiation (an advantage in terms of the probability of intercept of the radar waveform by a third party). This concept involves a higher degree of cooperation among the radar sites than typical multistatic radar systems. As such, it has parallels with multiple-input multiple-output (MIMO) systems in wireless communications,

and subsequent publications have adopted the “MIMO radar” nomenclature for radar systems with cooperating transmitters [12]–[15].

In this article, a MIMO radar is defined broadly as a radar system employing multiple transmit waveforms and having the ability to jointly process signals received at multiple receive antennas. Elements of MIMO radar transmit independent waveforms result in an omnidirectional beampattern or create

diverse beampatterns by controlling correlations among transmitted waveforms [16]. A MIMO radar may be configured with its antennas co-located or widely distributed over an area. MIMO radar is an emerging concept, but it is already apparent that it has the potential to make important contributions to the radar field. In [13]

it is observed that MIMO radar has more degrees of freedom than systems with a single transmit antenna. These additional degrees of freedom support flexible time-energy management modes [14], lead to improved angular resolution [17], [18], and improve parameter identifiability [19]. With widely separated antennas, MIMO radar has the ability to improve radar performance by exploiting RCS diversity [20], handle slow moving targets by exploiting Doppler estimates from multiple directions [21], and support high resolution target localization [22].

MIMO radar with widely separated antennas is the topic of this article; a companion article discusses MIMO radar with co-located antennas. From a model point of view, widely separated antennas take advantage of the spatial properties of extended targets, while with co-located antennas, the target is modeled as a point with no spatial properties. Each configuration and model has its strengths and challenges. With co-located antennas, MIMO radars can mimic beamformers utilizing low probability of intercept (LPI) waveforms. Rather than focusing energy on a target, the transmitted energy is evenly distributed in space [12]. The loss of processing gain compared to conventional phased-array beamforming due to the uniform illumination is compensated by the gain in time, since a narrow beam does not need to be scanned [15]. MIMO spatial signatures in systems with co-located antennas can be exploited to estimate radar parameters (location, RCS) of multiple targets, but the ability to resolve targets is limited by the Rayleigh resolution limit of the transmit/receive arrays. Widely separated antennas support high resolution target localization, and by focusing on the effect of the channel, a bridge is extended between MIMO radar and MIMO communications.

MIMO systems have led to a revolution in wireless communications [23]. Recent publications (for example, [20] and references therein) indicate that one can exploit similar ideas in radar, suggesting interesting cross-fertilization of ideas between MIMO communications and MIMO radar. For quite some time, it has been understood that radar targets provide a rich scattering environment yielding 5–20 dB target RCS fluctuations, as

## SPATIAL MULTIPLEXING IN MIMO COMMUNICATIONS EXPRESSES THE ABILITY TO USE THE TRANSMIT AND RECEIVE ANTENNAS TO SET UP A MULTIDIMENSIONAL SPACE FOR SIGNALING.

illustrated in Figure 1 [26]. Such targets display essentially independent scattering returns when radiated from sufficiently different directions (see [20] for a mathematical illustration of this using a reasonable model). The premise of MIMO radar with widely separated antennas is that angular spread (RCS variations as a function of aspect) can be exploited to improve radar performance in a variety of ways. The parallel to MIMO communication is recognized in the similar roles that the transmission medium (channel) and target play in respectively, communication and radar. In other words, the target serves as the “channel” in the radar problem. For

example, combining target returns resulting from independent illuminations yields a diversity gain akin to the diversity gain obtained in the communication problem over fading channels when the data is transmitted through independent channels. Diversity gains are well understood in communications [24]. In radar, the idea is that any individual look at the target might have a small amplitude return with a significant probability, but by increasing the number of looks, the probability that all the looks have small amplitude returns can be made arbitrarily small. In [25] and some other publications, the nomenclature statistical has been used for MIMO radars that exploit a target’s spatial diversity.

Diversity gain is only one of two key gains that MIMO communications can provide. The other gain is called spatial multiplexing [23]. Spatial multiplexing in MIMO communications expresses the ability to use the transmit and receive antennas to

set up a multidimensional space for signaling. Then, by suitable techniques, it is possible to form uncoupled, parallel channels that enable the rate of communication to grow in direct proportion to the number of such channels. Similarly, in MIMO radar, a multidimensional signal space is created when the returns from multiple scatterers or targets combine to generate a rich backscatter. With proper design, transmit-receive paths can be separated and exploited for improving radar performance.

In communications, the key property that made MIMO such a successful concept has been the ability to substitute the spatial dimension for the bandwidth

resource. Narrowband MIMO communication systems perform like wideband systems without MIMO. In radar, bandwidth also plays an important role. Frequency diversity has been applied to decorrelate RCS response of complex targets, and high resolution location estimation is possible with wideband waveforms [26]. As discussed in the sequel in the section on high resolution mode, by exploiting the spatial dimension, MIMO radar with widely separated antennas may overcome bandwidth limitations and support high resolution target localization. At the same time, this type of MIMO radar has the challenge of time and/or phase synchronizing distributed systems, and needs to deal with ambiguities stemming from the large separation between sensors.

This article reviews some recent work on MIMO radar with widely separated antennas with the goal of elucidating key concepts, illustrating them by examples, and thus encouraging further research on this emerging technology. The MIMO radar concept is introduced and discussed in the context of other radar architectures. Examples of MIMO radar applications are presented in the section on MIMO radar applications, with concluding remarks following in the last section. A comment on notation: vectors are denoted by lower-case bold, while matrices use upper-case bold letters. The superscripts “T” and “†” denote the transpose and Hermitian operators, respectively. Locations in the x-y plane are denoted in upper-case  $X = (x, y)$ .

### MIMO RADAR CONCEPT

This section introduces the MIMO radar signal model, discusses conditions leading to RCS spatial diversity, and contrasts the architecture of MIMO radar with other multiple-element radars.

### SIGNAL MODEL

Assume a distributed target that consists of many, say  $Q$ , independent, isotropic scatterers located in a plane that also contains the transmit and receive antennas. The scatterers are located at coordinates  $X_q, q = 1, \dots, Q$ , where  $X_q = (x_q, y_q)$ . Figure 2 provides an illustration of the setup. In the figure, a distributed target is shown to comprise four scatterers. Each scatterer is represented by a circle to emphasize its isotropic

**IN THE EXTREME OF A SINGLE SPHERICAL SCATTERER WITH UNIFORM RCS AS A FUNCTION OF ANGLE, THERE ARE NO MULTIPLE SIGNALS THAT COMBINE TO CREATE THE FADING ELEMENTS OF THE CHANNEL MATRIX.**

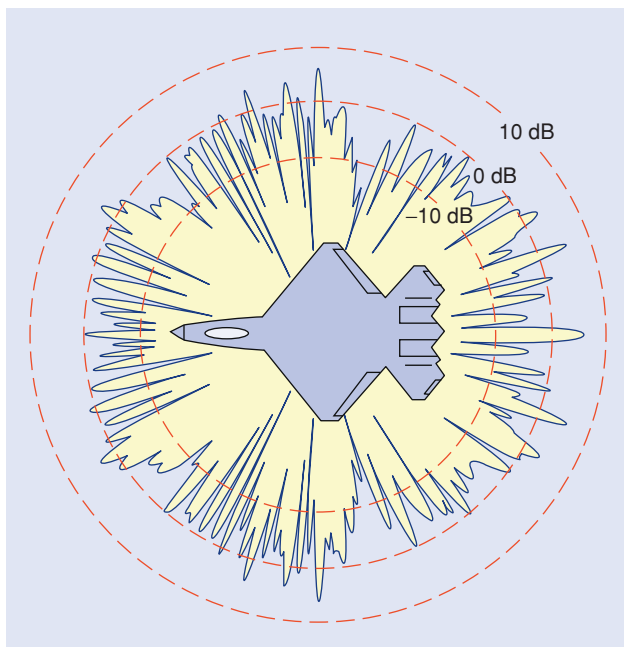


**[FIG1] Backscatter as function of azimuth.**

reflectivity. The reflectivity of a scatterer is modeled by a zero-mean, independent and identically distributed (i.i.d.) complex random variable  $\zeta_q$  with variance  $E[|\zeta_q|^2] = 1/Q$ . Reflectivity values of the target are organized in a diagonal  $Q \times Q$  matrix,  $\Sigma = \text{diag}(\zeta_1, \dots, \zeta_Q)$ . Given the reflectivity of an individual scatterer, the target average RCS is  $E[\text{tr}(\Sigma \Sigma^\dagger)] = 1$ , independent of the number of scatterers in the model. If the RCS fluctuations are fixed during an antenna scan, but vary independently from scan to scan, our target model represents a classical Swerling case I (which represents a target in slow motion) [26]. Now let the target be illuminated by  $M$  transmitters arbitrarily located at coordinates  $T_k = (x_{tk}, y_{tk})$ ,  $k = 1, \dots, M$ . The signals scattered by the target are collected by  $N$  sensors placed at arbitrary coordinates  $R_\ell = (x_{r\ell}, y_{r\ell})$ ,  $\ell = 1, \dots, N$ . The set of transmitted waveforms in lowpass equivalent form is  $\sqrt{E/M} s_k(t)$ ,  $k = 1, \dots, M$ , where  $\int_{\mathcal{T}} |s_k(t)|^2 dt = 1$ ,  $E$  is the total transmitted energy, and  $\mathcal{T}$  is the waveforms' duration. Normalization by  $M$  makes the total energy independent of the number of transmitters. Let all transmitted waveforms have the same bandwidth  $W$ . Then the two-dimensional resolution cells illustrated by the grid in Figure 2 have approximate dimensions  $(c/W) \times (c/W)$ , where  $c$  is the speed of light. Further specification of the waveforms  $s_k(t)$  depends on the application. For example, for focused beampatterns, the waveforms  $s_k(t)$  may be identical or differ by complex scalars. For target classification or parameter estimation, the statistical model for the observations may be employed for specialized waveform design [27]. In another example, for MIMO radar seeking to exploit target spatial diversity, it might be desired to design orthogonal waveforms, for ease of separation at the receiver. Orthogonality may be imposed in the time domain, frequency domain or in signal space. Throughout the article, it is assumed that transmitted waveforms are orthogonal and that orthogonality is maintained even for different mutual delays, i.e.,  $\int_{\mathcal{T}} s_k(t) s_m^*(t - \tau) dt = 0$  for all  $k \neq m$ , and for all time delays of interest.

In the model developed below, path loss effects are neglected, i.e., the model accounts for the effect of the sensors/target locations only through time delays (or phase shifts) of the signals. It is not difficult to show that the lowpass equivalent of the signal observed at sensor  $\ell$  due to a transmission from sensor  $k$  and reflection from a scatterer at coordinates  $X_q = (x_q, y_q)$  (and excluding noise) is given by

$$z_{\ell k}^{(q)}(t) = \sqrt{\frac{E}{M}} \zeta_q s_k(t - \tau_{tk}(X_q) - \tau_{r\ell}(X_q)) \times \exp(-j2\pi f_c[\tau_{tk}(X_q) + \tau_{r\ell}(X_q)]), \quad (1)$$

where  $\tau_{tk}(X_q) = d(T_k, X_q)/c$  is the propagation time delay between the  $k$ th transmitting sensor located at coordinates  $T_k$  and the scatterer at  $X_q$ ,  $d(T_k, X_q) = \sqrt{(x_{tk} - x_q)^2 + (y_{tk} - y_q)^2}$ , and  $f_c$  is the carrier frequency. The propagation time  $\tau_{r\ell}(X_q)$  from the scatterer to the  $\ell$ th receiving

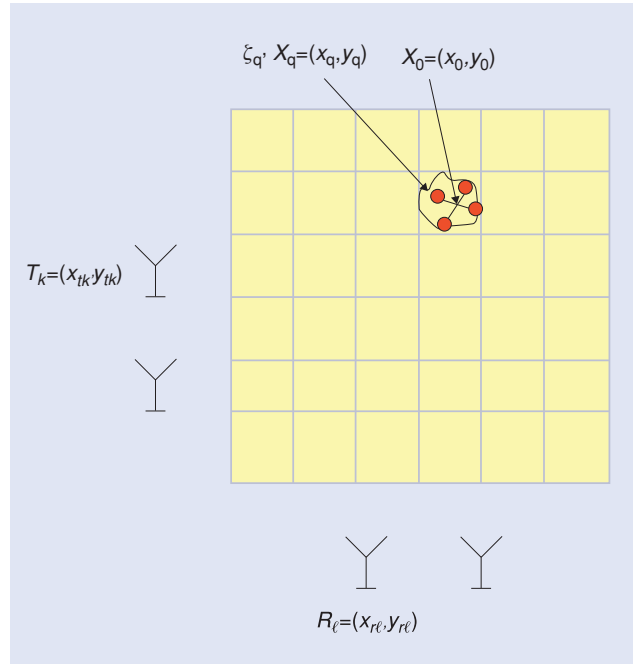


**[FIG2] MIMO radar with extended target. Target composed of four point scatterers. Scatterers located at points  $X_q$  and have reflectivity  $\zeta_q$ . RCS center of gravity located at  $X_0$ . Transmit antennas located at  $T_k$ , receive antennas located at  $R_\ell$ .**

sensor is defined analogously to  $\tau_{tk}(X_q)$ . Note that (1) denotes a near-field signal model, where the phase of the received signal is a function of the transmit and receive element locations as well as the location of the scatterer. In contrast, in a far-field signal model, the target is assumed to be sufficiently far such that it is essentially at the same distance and angle with respect to all the transmit and/or receive elements.

Continuing with the signal model in (1), we can interpret the term

$$h_{\ell k}^{(q)} = \zeta_q \exp(-j2\pi f_c[\tau_{tk}(X_q) + \tau_{r\ell}(X_q)]) \quad (2)$$

as the equivalent “channel” between transmitter  $k$ , scatterer  $q$ , and receiver  $\ell$ . A channel element (2) comprises three parts: i)  $\exp[-j2\pi f_c \tau_{tk}(X_q)]$ , the phase shift due to the propagation from transmitter  $k$  to scatterer  $q$ , ii)  $\zeta_q$ , the reflectivity of the scatterer, and iii)  $\exp[-j2\pi f_c \tau_{r\ell}(X_q)]$ , the phase shift due to the propagation from the scatterer to receiver  $\ell$ . Summing over all the scatterers that make up the target, the model in (3) becomes

$$z_{\ell k}(t) = \sqrt{\frac{E}{M}} \sum_{q=1}^Q h_{\ell k}^{(q)} s_k(t - \tau_{tk}(X_q) - \tau_{r\ell}(X_q)). \quad (3)$$

We assume that the bandwidth of the transmitted waveforms is such that they are not capable of resolving individual scatterers. This is stipulated by the condition that the target has an RCS center of gravity at  $X_0 = (x_0, y_0)$ , and that  $s_k(t - \tau_{tk}(X_q) - \tau_{r\ell}(X_q)) \approx s_k(t - \tau_{tk}(X_0) - \tau_{r\ell}(X_0))$  for all  $q = 1, \dots, Q$ . With this condition, (3) becomes

$$z_{\ell k}(t) = \sqrt{\frac{E}{M}} h_{\ell k} s_k(t - \tau_{tk}(X_0) - \tau_{r\ell}(X_0)), \quad (4)$$

where  $h_{\ell k} = \sum_{q=1}^Q h_{\ell k}^{(q)}$ .

The path gains  $h_{\ell k}$  from transmit to receive antennas of the MIMO radar are organized in a  $N \times M$  matrix  $\mathbf{H}$ . It can be shown that the matrix  $\mathbf{H}$  can be expressed [15]

$$\mathbf{H} = \mathbf{K}\Sigma\mathbf{G}. \quad (5)$$

Equation (5) highlights the contribution of the transmit paths, the target components, and the receive paths: The transmit paths are represented by the  $Q \times M$  matrix  $\mathbf{G}$ ,  $\mathbf{G} = [\mathbf{g}_1^T; \mathbf{g}_2^T; \dots; \mathbf{g}_Q^T]$ ,  $\mathbf{g}_q^T = [\exp[-j2\pi f_c \tau_{t1}(X_q)], \dots, \exp[-j2\pi f_c \tau_{tM}(X_q)]]$ . Information on the receive paths is embedded in the  $N \times Q$  matrix  $\mathbf{K}$ ,  $\mathbf{K} = [\mathbf{k}_1; \mathbf{k}_2; \dots; \mathbf{k}_Q]$ , the semi-colon separates rows, and  $\mathbf{k}_q^T = [\exp[-j2\pi f_c \tau_{r1}(X_q)], \dots, \exp[-j2\pi f_c \tau_{rN}(X_q)]]$ . We recall that the matrix  $\Sigma$  was defined in the section on signal model.

From (4) and accounting for additive noise, it is possible to express the observed waveforms at the receive antenna  $\ell$  as:

$$r_{\ell}(t) = \sqrt{\frac{E}{M}} \sum_{k=1}^M h_{\ell k} s_k(t - \tau_{tk}(X_0) - \tau_{r\ell}(X_0)) + w_{\ell}(t), \quad (6)$$

where  $w_{\ell}(t)$  is circularly symmetric, zero-mean, complex Gaussian noise, spatially and temporally white with autocorrelation function  $\sigma_w^2 \delta(\tau)$ . We define the vector  $\mathbf{r}(t) = [r_1(t), \dots, r_N(t)]^T$  for later use. Properties of the elements  $h_{\ell k}$  of the channel matrix  $\mathbf{H}$  are discussed next.

### SPATIAL DECORRELATION

In the previous subsection, we introduced a stochastic model for the channel elements  $h_{\ell k}$ . Here, we discuss the conditions for spatial decorrelation of these elements.

In [20], it is shown that, if  $Q$  is large, all the channel elements  $h_{\ell k}$  are jointly Gaussian with zero mean and unit variance. Let two transmit antennas have coordinates  $(x_{tk}, y_{tk})$  and  $(x_{ti}, y_{ti})$ , respectively, and let the target dimensions along the  $x$  and  $y$  axes be  $D_x$  and  $D_y$ , respectively. Furthermore, let two receive antennas have coordinates  $(x_{r\ell}, y_{r\ell})$  and  $(x_{rj}, y_{rj})$ , respectively. Recall the definitions of distance  $d(T_k, X_0)$  between transmit antenna at  $T_k$  and the target at  $X_0$ , and of distance  $d(R_{\ell}, X_0)$  between receiver antenna at  $R_{\ell}$  and the target at  $X_0$ . If at least one of the following four conditions are met:

$$\begin{aligned} \frac{x_{tk}}{d(T_k, X_0)} - \frac{x_{ti}}{d(T_i, X_0)} &> \frac{\lambda}{D_x} \\ \frac{y_{tk}}{d(T_k, X_0)} - \frac{y_{ti}}{d(T_i, X_0)} &> \frac{\lambda}{D_y} \\ \frac{x_{r\ell}}{d(R_{\ell}, X_0)} - \frac{x_{rj}}{d(R_j, X_0)} &> \frac{\lambda}{D_x} \\ \frac{y_{r\ell}}{d(R_{\ell}, X_0)} - \frac{y_{rj}}{d(R_j, X_0)} &> \frac{\lambda}{D_y} \end{aligned} \quad (7)$$

where  $\lambda$  is the carrier wavelength, then it is shown in [20] that the  $\ell k$ th and  $j i$ th elements of the channel matrix are *uncorrelated*. Conversely, if

$$\begin{aligned} \frac{x_{tk}}{d(T_k, X_0)} - \frac{x_{ti}}{d(T_i, X_0)} &\ll \frac{\lambda}{D_x} \\ \frac{y_{tk}}{d(T_k, X_0)} - \frac{y_{ti}}{d(T_i, X_0)} &\ll \frac{\lambda}{D_y} \\ \frac{x_{r\ell}}{d(R_{\ell}, X_0)} - \frac{x_{rj}}{d(R_j, X_0)} &\ll \frac{\lambda}{D_x} \\ \frac{y_{r\ell}}{d(R_{\ell}, X_0)} - \frac{y_{rj}}{d(R_j, X_0)} &\ll \frac{\lambda}{D_y} \end{aligned} \quad (8)$$

then the  $\ell k$ th and  $j i$ th elements of the channel matrix are correlated. Loosely speaking, these results mean that if the distributed target is viewed as an antenna with aperture length  $D$  ( $D$  could be  $D_x$  or  $D_y$  from the discussion above) the elements of the channel matrix  $\mathbf{H}$  decorrelate if the target's beamwidth cannot illuminate two sensors simultaneously. An illustration of this concept is shown in Figure 3. For example, for a target at distance  $d = 10^4 \lambda$  and of dimension  $D = 10 \lambda$ , the separation required between the elements of the MIMO radar is of the order  $10^3 \lambda$ . Conversely, when the distributed target acts as an antenna that has two sensors in the same beamwidth, elements of  $\mathbf{H}$  associated with these sensors are correlated. Since each element of  $\mathbf{H}$  represents the path gain of a transmitter-receiver pair, decorrelation supports a diversity of path gains. We conclude from the foregoing discussion that to obtain path diversity to an extended target, the MIMO radar antennas need to be sufficiently separated. However, even when the MIMO radar antennas are co-located, then decorrelation is still possible for large  $D$ . Taking the example we used earlier with a distance to target of  $d = 10^4 \lambda$ , the condition for decorrelation is  $D > 2 \times 10^4 \lambda$ , i.e., twice the distance to the target. In this case,  $D$  cannot be the aperture of a single extended target, but rather we could view two point targets separated by  $D$  as an array with two elements.

For further insight into the conditions for spatial decorrelation, let us consider the role of the target in the spatial decorrelation of the elements of  $\mathbf{H}$ . From the discussion so far, spatial decorrelation of the elements of the channel matrix occurs for complex targets (large number of scatterers  $Q$ ) and widely separated sensors. A large number of scatterers results in rich RCS patterns, such as the one in Figure 1. The large number of scatterers, each with its own reflectivity  $\zeta_q$  and location  $X_q = (x_q, y_q)$ , combine at the receive sensors to create a fading signal. Widely spaced sensors cause the paths from the transmitters ( $T_k$ 's in Figure 2) to the scatterers ( $X_q$ 's), and from the scatterers to the receivers ( $R_{\ell}$ 's) to be sufficiently diverse such that each receive sensor experiences a different fading signal. This is the root of the spatial decorrelation. What happens for simple targets with only a few scatterers? In the extreme of a single spherical scatterer with uniform RCS as a function of angle, there are no multiple signals that combine to create the fading elements of the channel matrix. With the loss of fading, the elements of the channel matrix become correlated.

## OTHER MULTIPLE ANTENNA RADARS

To gain additional insight into the MIMO radar signal model, we discuss here its relation to other multiple antenna radar systems.

### CONVENTIONAL PHASED-ARRAY RADAR:

In conventional array radar, the antennas are co-located, and the inter-element spacing is  $\lambda/2$ . Typically, the target is in the far-field of the antenna array, meaning that all antenna elements are at essentially the same distance and angle with respect to the target. In this case, it is easy to verify that the matrix  $\mathbf{G}$  defined earlier and representing the propagation from the transmit antennas to the target, can be expressed  $\mathbf{G} = \mathbf{1}_Q \otimes \mathbf{b}^T(\theta'_0)$ . Here  $\mathbf{1}_Q$  is a column vector of ones, the binary operation is the Kronecker product, and  $\mathbf{b}(\theta'_0)$  is a  $M \times 1$  vector representing the propagation from the transmit antennas to any of the scatterers that make up the target, when the target is at angle  $\theta'_0$  with respect to the normal to the transmit array ( $k$ th element is  $b_k(\theta'_0) = \exp[-j2\pi(k-1)\Delta_t \sin(\theta'_0)/\lambda]$ ). Similarly, the propagation paths from the target to the receive antennas are represented by the matrix  $\mathbf{K} = \mathbf{a}(\theta_0) \otimes \mathbf{1}_Q^T$ , where  $\mathbf{a}(\theta_0)$  is a  $N \times 1$  vector with components  $a_\ell(\theta_0) = \exp[-j2\pi(\ell-1)\Delta_r \sin(\theta_0)/\lambda]$ . Applying (5), it follows that the channel matrix  $\mathbf{H}$  equals

$$\mathbf{H} = \mathbf{K}\Sigma\mathbf{G} = \mathbf{a}(\theta_0)\mathbf{b}^T(\theta'_0) \sum_q \zeta_q. \quad (9)$$

Let the random variable  $\alpha = \sum_q \zeta_q$ . Then, for large  $Q$ , by the central limit theorem,  $\alpha$  is a zero-mean, variance 1, complex Gaussian random variable.

In phased-arrays, the same waveform  $s(t)$  is transmitted by all the antennas. To steer the transmitted beam in direction  $\theta'$  with respect to the transmit array, a steering vector  $\mathbf{b}^*(\theta')$  is applied such that  $s_k(t) = s(t)b_k^*(\theta')$ , where  $b_k^*(\theta') = \exp[j2\pi(k-1)\Delta_t \sin(\theta')/\lambda]$ . The assumption that the transmit and receive antennas are at the same distance  $d$  from the target implies that  $s_k(t - \tau_{tk}(X_0) - \tau_{r\ell}(X_0)) = s_k(t - \tau)$  for some  $\tau$ , and for all  $k$  and  $\ell$ . The received signal in (6) becomes

$$r_\ell(t) = \sqrt{\frac{E}{M}} \alpha a_\ell(\theta_0) \sum_{k=1}^M b_k(\theta'_0) b_k^*(\theta') s_k(t - \tau) + w_\ell(t). \quad (10)$$

Beamforming at the receiver in the direction  $\theta_0$ , we obtain at the output of the beamformer  $r(t) = \sum_{\ell=1}^N a_\ell^*(\theta_0) r_\ell(t)$ , which is the model for the received signal in conventional array radars [26].

### ADAPTIVE RADAR/STAP

There are two variations of phased-array radar that have been extensively studied in the literature: adaptive radar [5] and space-time adaptive radar (STAP) [6], [7]. In adaptive radar, the

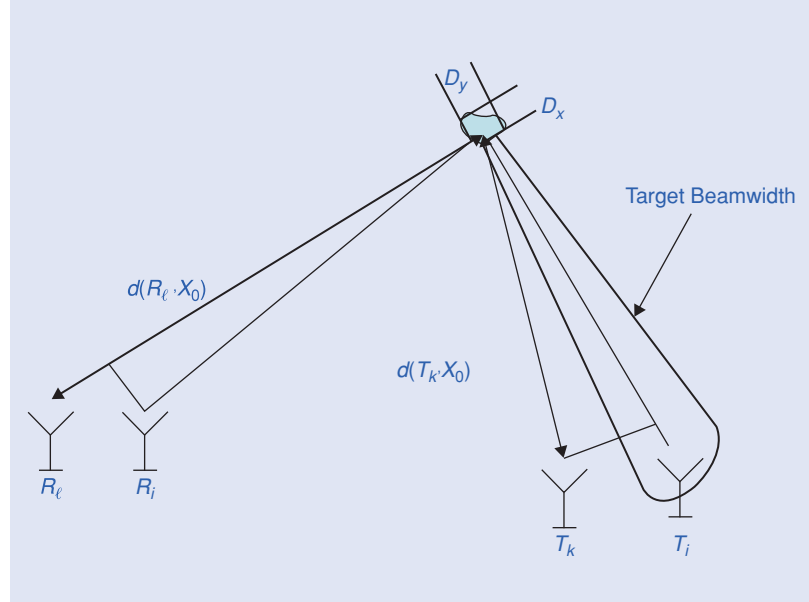


**[FIG3]** Elements of the channel matrix decorrelate when the MIMO radar antennas fall in different beamwidths originating from the target.

output is given by  $r(t) = \sum_{\ell=1}^N v_\ell^* r_\ell(t)$ , where  $v_\ell$  are weights computed based on some optimality criterion, such as maximizing the signal-to-interference ratio. STAP is an extension of adaptive radar that incorporates time domain as well as spatial domain processing. The STAP filter exploits spatial and time correlations to suppress clutter and interference (including jammers) and to detect moving targets.

### MULTISTATIC RADAR

Often the literature on bistatic/multistatic radars assumes that the individual radars that make up the system operate independently [28]. Detection, target estimation, and other high level products of local processing are communicated to a central processor. The preprocessing limits the amount of information that needs to be passed on to develop a final detection decision or estimation. The central processor takes advantage of the information delivered by each radar to improve detection/estimation performance [10], [29]–[31]. While in a general sense MIMO radar can be viewed as a type of multistatic radar, the different designation distinguishes it from the multistatic radar literature by emphasizing the joint processing of signals for transmission and reception, and the links to MIMO communications.

### MIMO RADAR APPLICATIONS

This section provides several examples of MIMO radar applications, which illustrate various aspects and properties of MIMO radar. The first example illustrates the application of MIMO radar to obtain a diversity gain to overcome fades in target RCS. In the second example, multistatic observations are exploited to improve the detection capability of a moving target. The final example exploits coherent processing among the elements of MIMO radar to obtain high resolution target detection/estimation.

## DIVERSITY GAIN

This subsection addresses radar functions that exploit RCS spatial diversity of targets. Diversity gains for target detection and direction finding are reviewed based on [20] and [33], respectively. In both cases, the target is stationary and it is observed against a background of white Gaussian noise.

## TARGET DETECTION

Diversity processing seeks to exploit multiple paths through which the signals propagate from the transmit antennas to the receive antennas. Such a path starts from a transmitter. The transmitted waveform impinges on the  $Q$  scatterers that form the target. The path terminates at a receiver, where the responses from the  $Q$  scatterers combine. Since the scatterers are too close to be resolved by the waveform, the  $Q$  echoes combine as in a flat fading multipath scenario to form a fading channel coefficient. With  $M$  transmit and  $N$  receive antennas, there are  $MN$  such paths corresponding to the  $MN$  elements of the channel matrix  $\mathbf{H}$ . Under the conditions discussed in the section on spatial decorrelation (complex targets with large  $Q$  and sufficiently spaced antennas) the  $MN$  paths are decorrelated. The set of transmitted waveforms has to be designed to facilitate the separation between waveforms arriving simultaneously at the receiver. Simple signal separation is possible when the transmitted waveforms are orthogonal and maintain their orthogonality at the receiver end.

For the target detection, we form two hypotheses: under hypothesis  $H_1$ , a target is present at  $X = (x, y)$ ; under the alternative hypothesis, the target is not present. The classic Neyman-Pearson detector is given by the likelihood ratio test

$$\log \frac{p_X(\mathbf{r}|H_1)}{p_X(\mathbf{r}|H_0)} \underset{H_0}{\overset{H_1}{\geq}} \gamma, \quad (11)$$

where  $p_X(\mathbf{r}|H_1)$  and  $p_X(\mathbf{r}|H_0)$  are the likelihood functions of the observation vectors under the respective hypotheses. The likelihood functions are parameterized by the location  $X$  of the resolution cell under test. The threshold  $\gamma$  is determined by the tolerated level of false alarms. Assuming that the components of the received vector  $\mathbf{r}(t)$  have bandwidth  $W$  (the same bandwidth as the transmitted waveforms), the density functions  $p_X(\mathbf{r}|H_1)$ ,  $p_X(\mathbf{r}|H_0)$  are understood in the conventional sense as joint distributions of samples of the real and imaginary parts of  $\mathbf{r}(t)$  taken at  $1/W$  time intervals (see for example [32]). From the signal model (6), the observations  $r_\ell(t)$  are functions of the channel coefficients  $h_{\ell k}$ . Concatenating the columns of the channel matrix  $\mathbf{H}$  to form the length  $MN$  vector  $\mathbf{h}$ , and recalling the discussion in the section on spatial decorrelation,  $\mathbf{h}$  is stochastic with probability density function  $p(\mathbf{h}) \propto \exp(-\|\mathbf{h}\|^2)$ , where  $\|\cdot\|$  denotes the Euclidean norm. This follows since the elements of  $\mathbf{h}$  are mutually independent with each element being complex Gaussian with zero mean and variance 1. The target detection process involves the simultaneous transmission of orthogonal waveforms and the testing of a decision statistic

by a central processor. The central processor is fed with data filtered and sampled by the receivers at delays corresponding to resolution cells. By suitable control of sampling instants, this process can test for the presence of a target in each of the resolution cells in Figure 2.

Assuming orthogonality between waveforms and the signal model in (6), it is possible to extract a noisy estimate of each element of  $\mathbf{H}$  corresponding to a point  $X = (x, y)$  in the  $x$ - $y$  plane. The estimate for element  $h_{\ell k}$  is obtained by applying the matched filter for waveform  $s_k(t)$  to the received signal at the  $\ell$ th antenna,  $r_\ell(t)$ , and sampling at a time delay corresponding to location  $X$ :

$$y_{\ell k}(X) = \int_{\mathcal{T}} r_\ell(t) s_k^*(t - [\tau_{tX}(X) + \tau_{r\ell}(X)]) dt. \quad (12)$$

Notice that by exploiting orthogonality between the transmitted waveforms,  $y_{\ell k}(X)$  contains the target response to  $s_k(t)$  only. Let  $\mathbf{y}(X)$  denote the vector formed by  $y_{\ell k}(X)$  for  $\ell = 1, \dots, N$  and  $k = 1, \dots, M$ . Starting with (6) and given the just described distribution for  $\mathbf{h}$ , it is possible to develop an expression for the probability density function of the received vector from a resolution cell containing the target and averaged over the values of  $\mathbf{h}$ . The detailed steps are omitted here due to space considerations, but following steps similar to those in [20], it can be shown that

$$\begin{aligned} p_X(\mathbf{r}|H_1) &= \int_{\mathbf{h}} p_X(\mathbf{r}|H_1, \mathbf{h}) p(\mathbf{h}) d\mathbf{h} \\ &\propto \exp \left[ -\frac{1}{\sigma_w^2} \left( \int_{\mathcal{T}} \|\mathbf{r}(t)\|^2 dt \right) \right] \\ &\quad \exp \left[ \frac{\|\mathbf{y}(X)\|^2}{\sigma_w^2 \left( \sigma_w^2 + \frac{E}{M} \right)} \right]. \end{aligned} \quad (13)$$

For hypothesis  $H_0$ , we have

$$p(\mathbf{r}(t)|H_0) \propto \exp \left[ -\frac{1}{\sigma_w^2} \left( \int_{\mathcal{T}} \|\mathbf{r}(t)\|^2 dt \right) \right]. \quad (14)$$

It follows that the Neyman-Pearson detector is given by

$$\|\mathbf{y}(X)\|^2 \underset{H_0}{\overset{H_1}{\geq}} \gamma_1. \quad (15)$$

In order to set the value of the threshold  $\gamma_1$  for a tolerated level of false alarms, the central processor has to have full model knowledge, i.e., the values of waveform energy  $E$  and noise power  $\sigma_w^2$ . By inspection of (15), the optimal processor is a non-coherent combiner of the signals preprocessed by the sensors. With  $M$  transmitters and  $N$  receivers and under conditions discussed earlier,  $\|\mathbf{y}(X)\|^2$  is the sum of the magnitudes of  $MN$

uncorrelated noisy estimates of channel coefficients. When, with suitable normalization, a single term  $|y_{\ell k}(X)|^2$  has a  $\chi_2^2$  (chi-square with two degrees of freedom) distribution, the test statistic in (15) has the improved statistical properties of a  $\chi_{2MN}^2$  random variable.

Closed-form performance expressions are given in [20] for cases with full and partial model knowledge. The figure reproduced here is for the case that the signal energy and noise power level are known. Figure 4 illustrates the gains provided by MIMO radar (curves labeled “MIMO”) over a conventional phased-array radar (labeled “conv”). The curves in the figure represent the miss probability as a function of SNR for a fixed false alarm probability of  $10^{-6}$  and for various MIMO/phased-array configurations. The slopes of the MIMO curves clearly show diversity gains similar to those obtained in communications (compare to [24] for example). For a more extensive set of results we refer the reader to [20].

#### DIRECTION FINDING

Another application that can benefit from the diversity gain of MIMO radar is direction finding (DF). In this case, the target spatial diversity is supported by widely separated transmitters, while the receiving sensors are placed at  $\lambda/2$  intervals to enable unambiguous DF. Such a system is studied in [33]. Here, we reproduce some of the numerical results from [33]. The mean square error (MSE) of the maximum likelihood (ML) estimate of the angle of arrival is evaluated and plotted versus the SNR for various antenna configurations. Figure 5 shows the MSE for a number of transmit antennas  $M = 1, 2, 4,$  and  $16,$  respectively. The target is located at boresight,  $\theta = 0,$  and the phased array at the receiver utilizes  $N = 6$  elements. It is observed that the MSE for the single-antenna case,  $M = 1,$  is much larger than for  $M = 4$  or  $M = 16.$  MIMO radar transmit diversity with  $M = 4$  provides a gain of more than 20 dB for the same MSE.

#### MOVING TARGET DETECTION

Observing targets over wide angular sectors with a MIMO radar offers great benefits for Doppler processing and moving target detection (MTD). MIMO radar is particularly useful in some cases when the targets are difficult to distinguish from the background clutter. The enhanced MTD performance of MIMO radar stems from its distributed nature, which makes it possible to overcome typical problems that plague conventional or array radars such as targets with low radial velocities or blind speeds. Further, the joint processing of the received waveforms results in superior performance com-

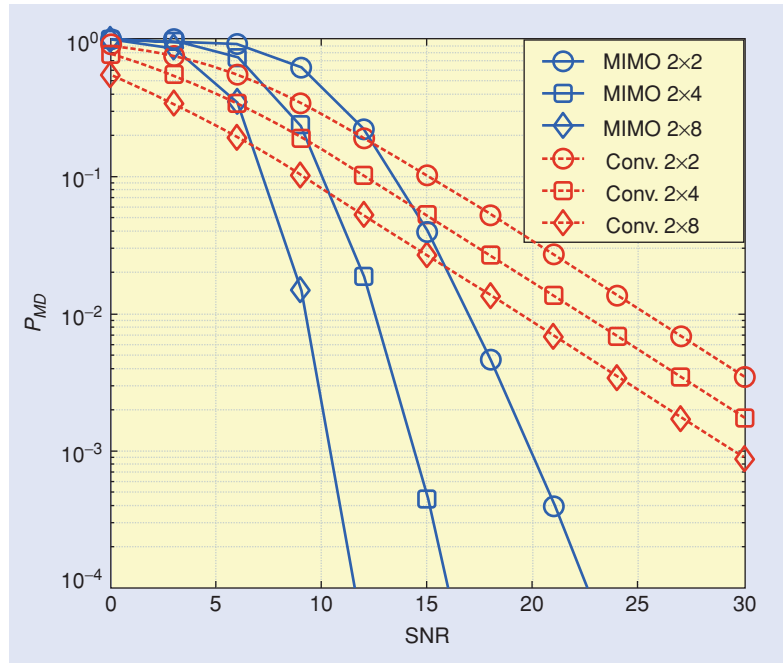


**[FIG4]** Miss probability of MIMO radar compared to conventional phased-array. Miss probability is plotted versus SNR for a fixed false alarm probability of  $10^{-6}$ .

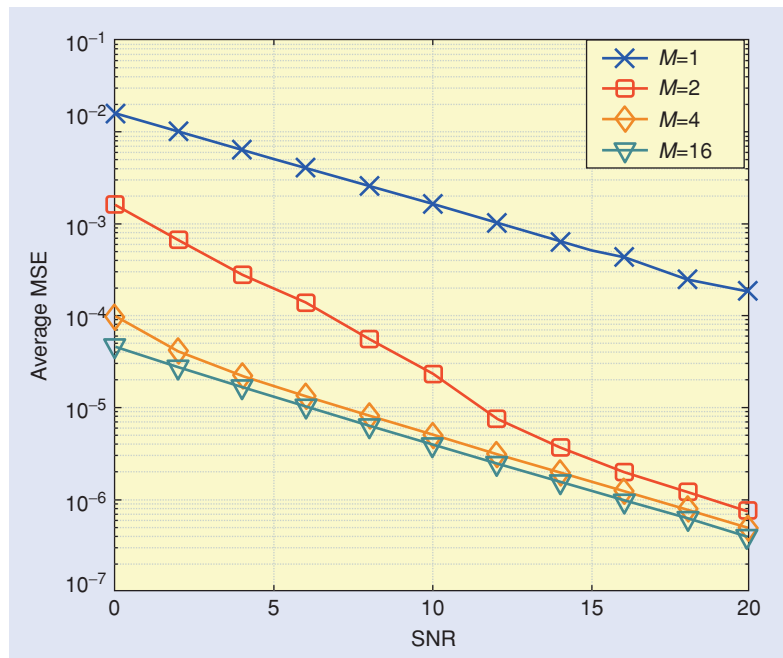


**[FIG5]** Average MSE of the ML estimator versus SNR.

pared to multistatic radar, referring here to the case where each sensor typically performs its own Doppler shift estimation.

MTD with MIMO radar is investigated in [21]. The scenario considered consists of a single transmitter and  $N > 1$  widely dispersed receivers. The transmitter and receivers are stationary. It is assumed that the moving target is sufficiently far from the sensors such that its Doppler shift with respect to the sensors is constant during the observation of  $K$  samples. A central

processor is fed with test statistics computed at the sensors. The clutter is assumed zero-mean, complex Gaussian with known  $K \times K$  temporal covariance matrix  $C$ . The clutter is also assumed spatially homogeneous in the sense that it has the same properties for all transmitter-receiver pairs and for all resolution cells. Previously, while discussing target detection, the channel elements  $h_{\ell k}$  were modeled as stochastic with known statistics. Here, we take a slightly different approach, and assume that these coefficients are deterministic unknown. The two slightly different approaches follow the respective models employed in the references that are reviewed in this article, but should not affect key features of MIMO radar.

In this subsection, tests for the detection of a single, moving target are discussed. The target, if present, is moving with unknown velocity components  $(v_x, v_y)$ , where  $v_x$  and  $v_y$  are deterministic, unknown velocities measured in an arbitrary Cartesian coordinate system (refer to Figure 6 for an illustration of the setup). Given  $M$  transmitters and  $N$  receivers, there are  $MN$  paths resulting in  $MN$  different spatial looks at the resolution cell under test. The same number of looks can be obtained with a single transmitter and  $MN$  receivers; hence, to simplify notation, and without loss of generality, the discussion below assumes  $M = 1$ . In Figure 6, the locations of the transmitter and the receiving sensors are denoted respectively,  $T_1$  and  $R_\ell$ ,  $\ell = 1, \dots, N$ . The target and the transmitter are aligned on the  $x$  axis, while the receivers form angles  $\theta_\ell$  with the target-transmitter axis.

To test for the presence of the target in a resolution cell, we develop a generalized likelihood ratio test (GLRT). The GLRT maximizes the likelihood ratio test over the unknown parameters: the target response  $h_{\ell k}$  and the velocities  $v_x, v_y$ . Under hypothesis  $H_1$ , a target is present in the tested resolution cell centered at coordinates  $X = (x, y)$ ; under the alternative hypothesis, the target is not present in the resolution cell. A vec-

tor  $y_\ell(X)$  is defined to consist of  $K$  time samples of the form  $y_{\ell 1}(X)$  defined in (12), and taken at the pulse repetition interval,  $T_{PRI}$ . The GLRT is evaluated by first expressing the likelihood ratio as a function of the unknown parameters  $h_{\ell k}, v_x$ , and  $v_y$ . Subsequently, the likelihood ratio is maximized over the unknown parameters. Skipping the details of the analysis, we list the MTD decision rules obtained for three types of radar: MIMO radar, distributed multistatic radar, and phased array radar:

The GLRT decision rule for MIMO radar is

$$\max_{v_x, v_y} \sum_{\ell=1}^N \frac{|\mathbf{d}^\dagger(f_\ell) \mathbf{C}^{-1} \mathbf{y}_\ell(X)|^2}{\mathbf{d}^\dagger(f_\ell) \mathbf{C}^{-1} \mathbf{d}(f_\ell)} \underset{H_0}{\overset{H_1}{\geq}} \gamma_2, \quad (16)$$

where  $\mathbf{d}(f_\ell)$  is a  $K \times 1$  vector representing the matched filter to a target response with Doppler frequency  $f_\ell$ . This vector is composed of  $K$  time samples taken at the pulse repetition intervals,  $T_{PRI}$ , and it has the form

$$\mathbf{d}(f_\ell) = [1, \exp[-j2\pi f_\ell T_{PRI}], \dots, \exp[-j2\pi f_\ell (K-1)T_{PRI}]]^T, \quad (17)$$

where  $f_\ell$  is the Doppler shift due to the motion between the sensor and the target. The Doppler shift can be evaluated with the help of Figure 6, and it is given by

$$f_\ell = \frac{v_x}{\lambda} (1 + \cos \theta_\ell) + \frac{v_y}{\lambda} \sin \theta_\ell. \quad (18)$$

For example, for a target moving along the  $x$  axis with velocity  $v_x$  towards the transmitter and receiver, the Doppler shift comprises the frequency shift due to the motion between transmitter and target ( $v_x/\lambda$ ), and the frequency shift due to the target-receiver motion ( $(v_x/\lambda) \cos \theta_\ell$ ). Finally, the threshold  $\gamma_2$  is determined by the tolerated level of false alarms. Notice that the test statistic in (16) is computed for each resolution cell  $X$  represented by a square in Figure 6. The location  $X$  of the resolution cell determines the values of angle  $\theta_\ell$  needed in (18) and the values of  $y_\ell(X)$  computed using (12). A test statistic is computed at each sensor such that the clutter spectrum is whitened. The optimal processor is a non-coherent combiner of the test statistics computed at each sensor. The aggregate statistic is maximized over values of  $v_x, v_y$  velocities and the result is compared to the threshold  $\gamma_2$  to decide on the target presence.

Moving on to the distributed multistatic radar, each sensor performs its own estimation of the Doppler shift  $f_\ell$  rather than the joint processing carried out by the

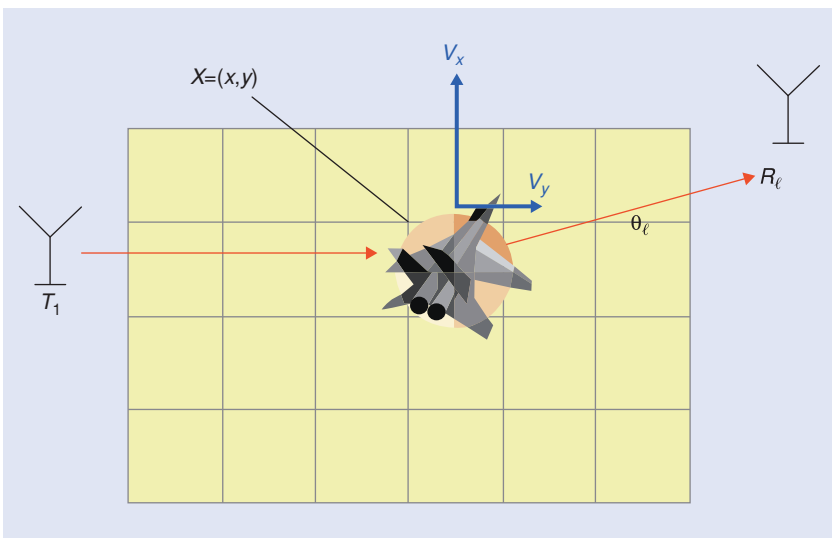


**[FIG6]** Moving target detection scenario: single transmit antenna at location  $T_1$ , multiple receive antennas at locations  $R_\ell$ , making angles  $\theta_\ell$ ,  $\ell = 1, \dots, N$ . Target at  $X = (x, y)$  with velocity components  $v_x, v_y$ .

MIMO radar. This means that rather than finding estimates  $v_x, v_y$  and restricting  $f_\ell$  to the form in (18), each sensor estimates  $f_\ell$  that maximizes a statistic computed locally. Then, the decision rule is

$$\sum_{\ell=1}^N \max_{f_\ell} \frac{|\mathbf{d}^\dagger(f_\ell) \mathbf{C}^{-1} \mathbf{y}_\ell(X)|^2}{\mathbf{d}^\dagger(f_\ell) \mathbf{C}^{-1} \mathbf{d}(f_\ell)} \underset{H_0}{\overset{H_1}{\geq}} \gamma_3, \quad (19)$$

where  $\mathbf{d}(f_\ell)$  is still defined by (17), but  $f_\ell$  does not have to obey (18).

Finally, the performance of the phased array is limited by its small aperture. Lacking the ability to view the target from multiple aspects, the phased array can observe only a single Doppler shift,  $f_\ell = f$ . The  $N$  transmit elements are beamformed to provide coherent processing gain. The GLRT decision rule is then given by

$$\max_f \frac{|\mathbf{d}^\dagger(f) \mathbf{C}^{-1} \mathbf{y}(X)|^2}{\mathbf{d}^\dagger(f) \mathbf{C}^{-1} \mathbf{d}(f)} \underset{H_0}{\overset{H_1}{\geq}} \gamma_4, \quad (20)$$

where  $\mathbf{y}(X)$  is the vector of  $K$  time samples at the output of the beamformed array corresponding to a target at  $X$ .

The receiver operating characteristics (ROC) of the three different types of radar systems: the MIMO radar from (16) (labeled “MIMO”), the distributed multistatic radar from (19) (“MS”), and the array radar from (20) (“conv”) are shown in Figure 7. Parameters used in the simulations include  $T_{\text{PRI}} = 0.5$  ms,  $K = 10$  samples, carrier frequency = 1 GHz, clutter-to-noise ratio = 30 dB, and target angle of arrival  $0^\circ$ . There are  $N = 8$  receiving sensors placed at uniformly spaced angles in the sector  $-40^\circ$  to  $50^\circ$  with respect to the target. The target velocity is 300 km/h with random direction. The curves are parameterized by the target-to-clutter ratio (“tc”).

The results demonstrate the advantage of MIMO radar for the chosen operational parameters. The advantage over distributed multistatic radar stems from the joint processing that constrains the search to velocities ( $v_x, v_y$ ) common to all sensors. An additional advantage of MIMO radar

is the ability to exploit the spatial diversity of RCS values. The multistatic radar can also benefit from RCS diversity, but since Doppler processing is local, it yields higher false alarms. The increase in false alarms accounts for the gap in performance. The phased-array radar is handicapped by both low Doppler response to low radial velocities and by RCS fading.

#### HIGH RESOLUTION MODE—COHERENT PROCESSING

It is useful at this point to review the time and phase synchronization requirements of the MIMO radar applications discussed in previous subsections. The processing for target detection with diversity gain is noncoherent. The computation of the statistic (15) with components given by (12) requires the adjustment of time delays. This means that sensors need to have a common time reference, but phase synchronization is not required. For the DF application, time synchronization is required between widely distributed transmitters, while the receive end operates as a phased-array with inter-element spacing of  $\lambda/2$ , and needs phase synchronization. The moving target detector requires time synchronization among sensors. In addition, each sensor is required to perform coherent time sampling. In the examples discussed so far, targets were extended (comprising multiple scatterers) and the transmit antennas sent orthogonal waveforms.

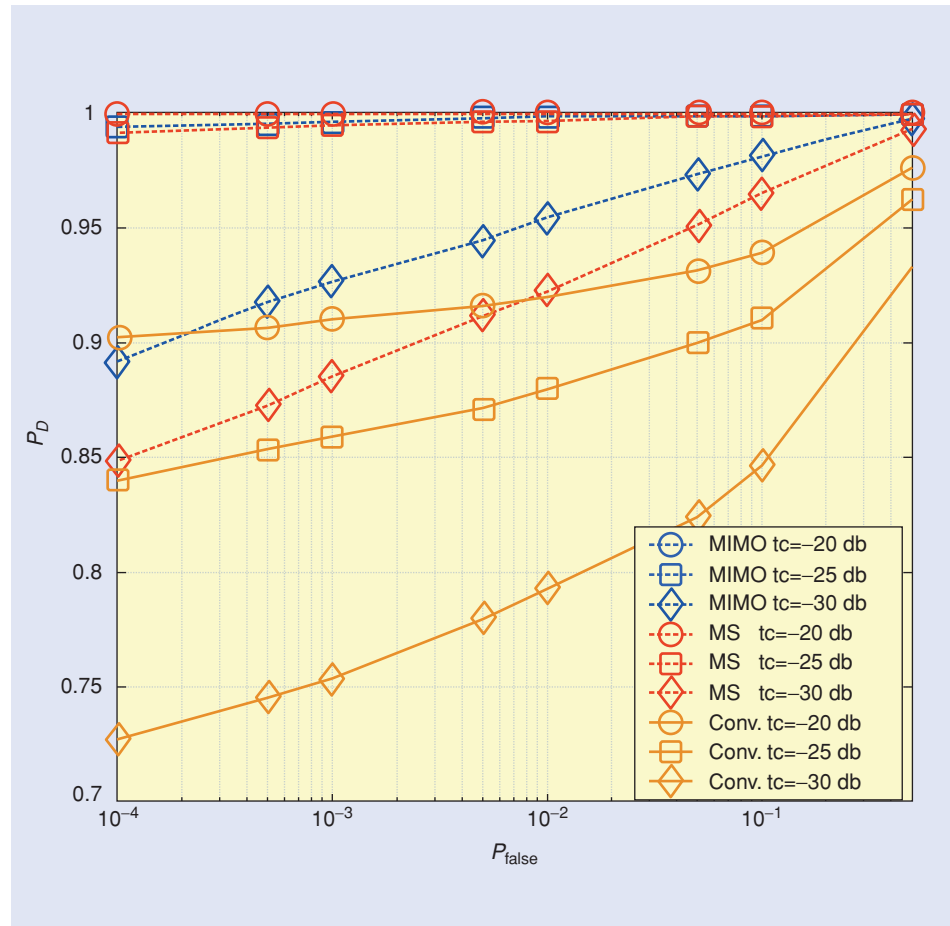


[FIG7] ROC for a 300 km/h target with random direction and with RCS fluctuations.

We now turn to applications that require phase synchronization among widely separated sensors. Phase synchronization is required at both the transmit and receive ends. In the first example, we discuss high resolution target localization. The second example is on the application of MIMO radar to estimate the number of targets.

We start by assuming a point target located at  $X_0 = (x_0, y_0)$ . The case of multiple targets will be discussed subsequently. From (6), we have

$$r_\ell(t) = \sqrt{\frac{E}{M}} \sum_{k=1}^M h_{\ell k} s_k(t - \tau_{tk}(X_0) - \tau_{r\ell}(X_0)) + w_\ell(t), \quad (21)$$

where the term  $h_{\ell k}$  is of the form (2), i.e.,  $h_{\ell k} = \zeta_0 \rho_{\ell k}(X_0)$ , and  $\rho_{\ell k}(X_0) = \exp[-j2\pi f_c(\tau_{tk}(X_0) + \tau_{r\ell}(X_0))]$ . The notation  $\rho_{\ell k}(X_0)$  emphasizes the dependency of the channel on the location of the target. The quantity  $\zeta_0$  represents the isotropic reflectivity of the target. In the discussion on diversity gain, the target comprised multiple scatterers, and the central limit theorem was invoked to associate a probability distribution with the target. Here, we assume that the target comprises a single scatterer, and that its reflectivity is  $\zeta_0$ . The reflectivity  $\zeta_0$  can be modeled as a random variable similar to the section on diversity gain or as an unknown deterministic quantity as in the section on moving target detection. Following [22], the latter model is assumed for  $\zeta_0$ .

For high resolution target detection, we can set up a log-likelihood ratio test such as in (11), except that the likelihoods are calculated assuming the model for  $h_{\ell k}$  laid out in the previous paragraph. First, we develop the test statistic, then, we will demonstrate that the cells are of higher resolution than the detector (15). Under the  $H_1$  hypothesis, the likelihood function conditioned on the reflectivity  $\zeta_0$  and computed for a point  $X = (x, y)$  is given by

$$\begin{aligned} p_X(\mathbf{r}|H_1, \zeta_0) \propto \exp \left( -\frac{1}{\sigma_w^2} \sum_{\ell=1}^N \int_{\mathcal{T}} |r_\ell(t) \right. \\ \left. - \zeta_0 \sqrt{\frac{E}{M}} \sum_{k=1}^M \rho_{\ell k}(X) s_k(t - \tau_{tk}(X) \right. \\ \left. - \tau_{r\ell}(X)) \right|^2 dt \Big). \end{aligned} \quad (22)$$

The likelihood (22) is conditioned on  $\zeta_0$ . Keeping only terms that are dependent on the location  $X$

$$\begin{aligned} p_X(\mathbf{r}|H_1, |\zeta_0|) \propto \exp \left( -\frac{\sqrt{E}}{\sigma_w^2} \left[ |\zeta_0|^2 \sqrt{\frac{E}{M}} MN \right. \right. \\ \left. \left. - 2\text{Re} \left( \zeta_0^* \sum_{\ell=1}^N \sum_{k=1}^M \rho_{\ell k}^*(X) y_{\ell k}(X) \right) \right] \right) \end{aligned} \quad (23)$$

where  $(\text{Re}\{\cdot\})$  denotes the real part) and  $y(X)$  was defined in (12). To get rid of the nuisance parameter  $\zeta_0$ , its MLE is calculated and substituted back in (23). From (23), the MLE of  $\zeta_0$  is given by

$$\hat{\zeta}_0 = \frac{1}{\sqrt{\frac{E}{M}} MN} \sum_{\ell=1}^N \sum_{k=1}^M \rho_{\ell k}^*(X) y_{\ell k}(X).$$

Substituting back in (23) and dividing by  $p_X(\mathbf{r}|H_0) \propto \exp(-\frac{1}{\sigma_w^2} \sum_{\ell=1}^N \int_{\mathcal{T}} |r_\ell(t)|^2 dt)$ , it can be shown that the log-likelihood is given by

$$L_X(\mathbf{r}) \propto \left| \sum_{\ell=1}^N \sum_{k=1}^M \rho_{\ell k}^*(X) y_{\ell k}(X) \right|^2. \quad (24)$$

This expression must be evaluated by a central processor and it requires phase synchronization across both transmit and receive sensors. This is in contrast with the processing that extracts diversity gains or performs moving target detection, where the processing across sensors was non-coherent.

To obtain further insight into the high resolution mode, focus on the noiseless part of  $L_X(\mathbf{r})$ , and define the function

$$A(X) = \frac{1}{MN} \left| \sum_{\ell=1}^N \sum_{k=1}^M \rho_{\ell k}^*(X) \varphi_{\ell k}(X) \right|^2, \quad (25)$$

where

$$\varphi_{\ell k}(X) = \int_{\mathcal{T}} s_k(t) s_k^*(t - \tau_{tk}(X) - \tau_{r\ell}(X)) dt. \quad (26)$$

The function  $A(X)$  represents the zero Doppler cut through the ambiguity function. The ambiguity function represents the response to a point target of reflectivity  $\zeta_0 = 1$  located at  $X_0$ , when the processing is adapted to a target located at  $X$ . The term  $\varphi_{\ell k}(X)$  is the ambiguity function (zero-Doppler cut) of the transmitted waveform measured at sensor  $\ell$ . Since  $A(X)$  requires phase information, it is referred to as the coherent ambiguity function of the MIMO radar. The high resolution properties of  $A(X)$  are determined by the phase terms  $\rho_{\ell k}(X) = \exp(j2\pi f_c[(\tau_{r\ell}(X) - \tau_{r\ell}(X_0))])$ . The noncoherent ambiguity function (assuming a point target) is given by

$$A_{nc}(X) = \frac{1}{MN} \left| \sum_{\ell=1}^N \sum_{k=1}^M \varphi_{\ell k}(X) \right|^2. \quad (27)$$

It is clear that the values of the coherent ambiguity function are upper bounded by the noncoherent ambiguity function  $A(X) \leq A_{nc}(X)$ . The ‘‘coherent’’ ambiguity function  $A(X)$  is plotted in Figure 8 for a  $9 \times 9$  system and for the  $x$  coordinate. The ‘‘noncoherent’’ ambiguity function  $A_{nc}(X)$  is shown for

comparison. The transmitters and receivers are placed uniformly in the sector  $-45^\circ$  to  $45^\circ$  with respect to the target. The ratio between the bandwidth and the carrier frequency is 0.01 (see [34] for more details). The high resolution capability is evident in the fact that the width of the mainlobe of the coherent ambiguity function is approximately equal in size to the wavelength  $\lambda$ , while the mainlobe of the noncoherent ambiguity function (determined by the bandwidth) is much wider.

The discussion above was concerned with a high resolution mode of MIMO radar applied to a point target. High resolution processing can also be applied to more complex settings. Next, we demonstrate the ability of MIMO radar for resolving four targets located at coordinates  $(0, 0)$ ,  $(0, 6\lambda)$ ,  $(6\lambda, 0)$ , and  $(6\lambda, 6\lambda)$ , respectively. Figure 9 is a three-dimensional representation of the ambiguity function for four targets [34]. To compute the ambiguity function for this case, the first  $s_k(t)$  in (26) is substituted with  $\sum_{k=1}^4 s_k(t - \tau_{tk}(X_k) - \tau_{rl}(X_k))$ , where the  $X_k$ 's represent the targets' locations. The four targets are clearly visible.

The high resolution mode enabled by the coherent processing of widely distributed sensors merits further discussion. It is well known that given a linear array of length  $L$ , fully populated with sensors spaced at  $\lambda/2$  intervals, the cross-range resolution (the dimension parallel to the array) at distance  $d$  from the array is approximately  $\delta = d\lambda/L$ . Thinning the array preserves the resolution, but gives rise to grating lobes. Randomly placing the sensors of the thinned array breaks up the grating lobes at the cost of higher sidelobes than the fully populated array. Such arrays are referred to as random arrays and their properties have been investigated [35], [36]. Statistical analysis for a single transmitter and  $N$  receivers has shown that the mean sidelobe level (MSL) is approximately  $1/N$ . Our formulation of MIMO radar leading to (24) is consistent with an extension of the linear random array concept to a planar topology and multiple transmitters. The resolution of MIMO radar configured with widely separated elements scales with the carrier wavelength  $\lambda$ , and thus, can greatly exceed the bandwidth resolution barrier set by the radar illuminating waveform.

With the higher resolution, the number of tests required for target detection may increase dramatically. An efficient mode of operation could be to let MIMO radar first detect the target over resolution cells  $(c/W) \times (c/W)$  using the techniques discussed in the section on diversity gains. Once the presence of a target is determined, the MIMO radar will switch to high resolution mode

seeking to extract additional information such as high resolution location, size, identification, etc.

While the MSL can be controlled through the number of elements in the array, more troubling from a performance point of view is the peak sidelobe level (PSL), which can exceed the MSL by 10 dB or more [35]. Controlling the MSL and PSL is of great

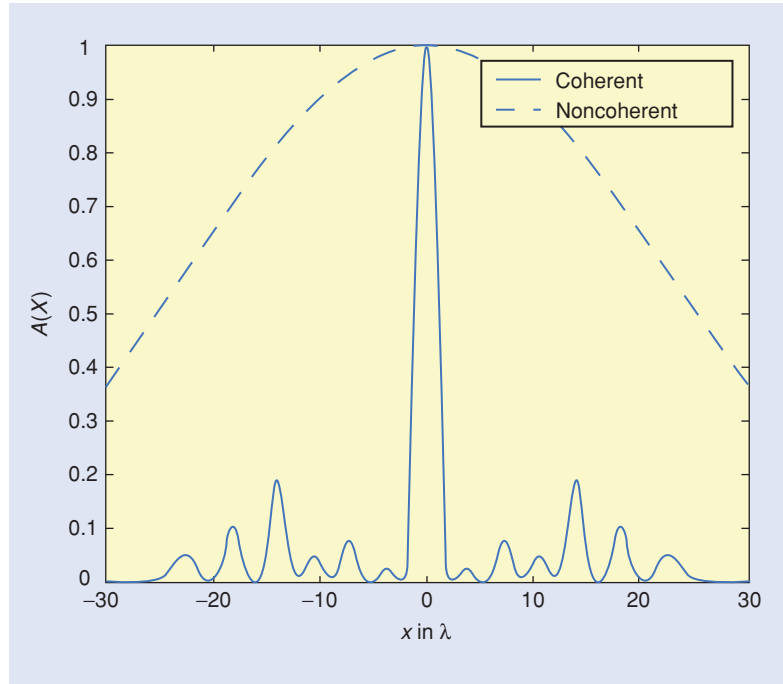


**[FIG8] Coherent and noncoherent ambiguity functions for a  $9 \times 9$  MIMO radar system.**

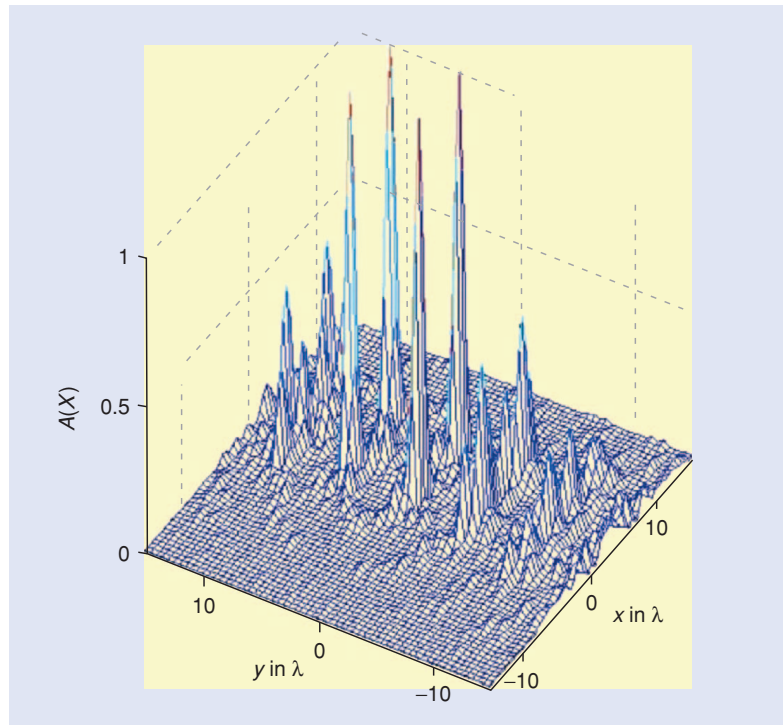


**[FIG9] Coherent ambiguity function of a  $9 \times 9$  MIMO radar for four targets.**

interest in high resolution applications of MIMO radar. Maintaining coherency across sensors at both the transmit and receive ends results in a MSL of the order of  $1/(MN)$ . Note that a MIMO radar with full coherency requires  $(M + N)$  sensors to achieve the same MSL as a radar with one transmitter and  $MN$  receivers. MIMO radar thus has an economical advantage, since for cases of interest,  $(M + N) \ll MN$ .

A variety of techniques are available for reducing the PSL. Waveforms with frequency diversity were suggested in [36]. Another idea first mentioned in the context of linear random arrays and that seems to have a natural extension to MIMO radar is the noncoherent combining of several random arrays [36].

#### “SPATIAL MULTIPLEXING” WITH MIMO RADAR

Using the signal model developed in the section on MIMO radar concept, the number of targets that can be handled simultaneously parallels the concept of “spatial multiplexing” in communications. The rank of the

matrix  $\mathbf{H}$  defined in (5) is upper bounded by the lowest rank among the matrices  $\mathbf{K}$ ,  $\Sigma$ , and  $\mathbf{G}$ . For sufficiently separated receive antennas, it can be shown that  $\text{rank } \mathbf{K} = N$  [15], [20]. Similarly, for sufficiently separated transmit antennas,  $\text{rank } \mathbf{G} = M$ . Finally, for  $Q$  point targets present,  $\text{rank } \Sigma = Q$ . If  $Q \leq \min(M, N)$ , the rank of the matrix  $\mathbf{H}$  serves as an indicator of the number of targets in the field of view of the MIMO radar. An estimate of  $Q$  can be determined efficiently from a singular value decomposition of  $\mathbf{H}$  provided that the magnitudes of the singular values of the noise-plus-clutter are known to be much smaller than those corresponding to the signal returns.

#### CONCLUSIONS

In this article, we introduced the concepts of MIMO radar and reviewed some recent work focusing on applications with widely dispersed antenna elements. Generally speaking, MIMO radars transmit multiple waveforms, receive signals at multiple antennas, and process them jointly. Processing may be carried out noncoherently or coherently.

The main topics discussed in this article can be summarized as follows:

- Complex targets contain a large number of scatterers that result in diverse RCS patterns as a function of angle. Decorrelation of the elements of the channel matrix occurs for complex targets and widely separated antennas.
- For a target with spatially diverse backscatter, optimal processing of MIMO radar with suitably located sensors leads to diversity gains in the form of improved statistics of the SNR. The processing collects the energy reflected by the scatterers and combines it noncoherently.
- MIMO radar can locate targets with high resolution and can resolve between closely spaced targets. The processing for

high resolution location beamforms the transmitted and the received signals to achieve resolution on the scale of the carrier wavelength. High resolution target localization is challenged by ambiguity sidelobes and the need to phase synchronize a distributed radar system.

- MIMO radar with a hybrid architecture of widely distributed transmitting sensors and a phased array receiver provides diversity gains for direction finding.
- Observations over a wide angular sector can be exploited to detect targets moving in arbitrary directions.

MIMO radar with widely separated sensors is a very promising concept for future, high performance radars. Yet many research and engineering challenges need to be addressed to advance MIMO radar from concept to reality. Engineering challenges include: centralized coordination of sensor transmissions, synchronized communication with a processing center, and highly precise phase synchronization among sensors (of the order of nanoseconds for

resolutions in meters). Research challenges include a better understanding of bistatic and multistatic RCS phenomena, tracking targets with MIMO radar, MIMO radar on airborne platforms, and others.

#### ACKNOWLEDGMENTS

The authors would like to thank Dr. Nikolaus Lehmann for his help in running simulations and generating some of the figures in the article. The work of Alexander Haimovich was supported in part by the Air Force Research Laboratory under agreement No. FA9550-06-1-0026. The work of Rick S. Blum was supported by the Air Force Research Laboratory under agreement No. FA9550-06-1-0041.

#### AUTHORS

*Alexander M. Haimovich* (haimovic@njit.edu) is a professor of electrical and computer engineering at the New Jersey Institute of Technology. He recently served as the Director of the New Jersey Center for Wireless Telecommunications, a state funded consortium including NJIT, Princeton University, Rutgers University, and Stevens Institute of Technology. He has been at NJIT since 1992. Prior to that, he served as Chief Scientist of JJM Systems from 1990 until 1992. From 1983–1990 he worked in a variety of capacities, up to senior staff consultant, for AEL Industries, Lansdale, Pennsylvania. He received the Ph.D. degree in systems from the University of Pennsylvania in 1989, the M.Sc. degree in electrical engineering from Drexel University in 1983, and B.Sc. degree in electrical engineering from the Technion, Haifa, Israel in 1977. His research interests include MIMO systems, wireless networks, array processing for wireless communication, and radar. He is a Senior Member of the IEEE.

**MIMO RADAR WITH A HYBRID ARCHITECTURE OF WIDELY DISTRIBUTED TRANSMITTING SENSORS AND A PHASED ARRAY RECEIVER PROVIDES DIVERSITY GAINS FOR DIRECTION FINDING.**

**Rick S. Blum** (rblum@eecsl.lehigh.edu) received a Ph.D. in electrical engineering from the University of Pennsylvania and a B.S.E.E from Pennsylvania State University. Formerly with General Electric Aerospace, he is currently with the ECE Department at Lehigh University where he is a professor and holds the Robert W. Wieseman Chaired Professorship in Electrical Engineering. His research interests include communications, sensor networking, sensor processing, and related topics in the areas of signal processing and communications. He has been an associate editor for *IEEE Transactions on Signal Processing*, *IEEE Communications Letters* and *Journal of Advances in Information Fusion* as well as several special issues of various journals. He served on technical committees in both the Signal Processing and Communications Societies. He is a member of the awards committee of the IEEE Communication Society. He is a Fellow of the IEEE, an IEEE Third Millennium Medal winner, and an ONR Young Investigator Award winner.

**Leonard J. Cimini, Jr.** (cimini@ece.udel.edu) received a Ph.D. in electrical engineering from the University of Pennsylvania in 1982, and worked at AT&T, first in Bell Labs and then AT&T Labs, for twenty years. His research has concentrated on lightwave and wireless communications, in particular OFDM for high bit-rate applications. He was the founding editor-in-chief of the *IEEE J-SAC: Wireless Communications Series*. He is the chair of the Emerging Technologies Committee of ComSoc and an At-Large Member of the Board of Governors. He was elected a Fellow of the IEEE in 2000 for contributions to the theory and practice of high-speed wireless communications. He has been a professor in the Electrical and Computer Engineering Department at the University of Delaware since 2002.

## REFERENCES

- [1] E. Brookner, "Phase arrays around the world—Progress and future trends," in *Proc. IEEE Int. Symp. Phased Array Systems and Technology*, Oct. 2003, pp. 1–8.
- [2] L. Swindlehurst and P. Stoica, "Maximum likelihood methods in radar array signal processing," *Proc. IEEE*, vol. 86, pp. 421–441, Feb. 1998.
- [3] S. Haykin, J. Litva, and T.J. Shepherd, *Radar Array Processing*, 1st ed. New York: Springer-Verlag, 1993.
- [4] A. Farina, *Antenna Based Signal Processing Techniques for Radar Systems*, Norwood, MA: Artech House, 1992. Science Publishers, 1998.
- [5] L.E. Brennan and I.S. Reed, "Theory of adaptive radar," *IEEE Trans. Aerosp. Electron. Syst.*, vol. AES-9, pp. 237–252, Mar. 1973.
- [6] J. Ward, "Space-time adaptive processing for airborne radar," in *Proc. IEEE National Radar Conf.*, 1995, pp. 2809–2812.
- [7] W.L. Melvin, "A STAP overview," *IEEE Aerosp. Electro. Syst. Mag.*, vol. 19, pp. 19–35, Jan. 2004.
- [8] R. Klemm, *Principles of Space-Time Adaptive Radar*. London: IEE Press, 2002.
- [9] J.R. Guerci, *Space-Time Adaptive Processing for Radar*. Norwood, MA: Artech House, 2003.
- [10] V.S. Chernyak, *Fundamentals of Multisite Radar Systems*. New York: Gordon and Breach, 1998.
- [11] J.M. Colin, "Phased array radars in France: Present and future," in *Proc. IEEE Int. Symp. Phased Array Systems and Technology*, Oct. 1996, pp. 458–462.
- [12] A.S. Fletcher and F.C. Robey, "Performance bounds for adaptive coherence of sparse array radar," presented at *11th Conf. Adaptive Sensors Array Processing*, Mar. 2003 [Online]. Available: [http://www.11.mit.edu/asap/asap\\_03/6-page\\_papers/fletcherASAPpaper.pdf](http://www.11.mit.edu/asap/asap_03/6-page_papers/fletcherASAPpaper.pdf)
- [13] D.W. Bliss and K.W. Forsythe, "Multiple-input multiple-output (MIMO) radar and imaging: Degrees of freedom and resolution," in *Proc. 37th Asilomar Conf. Signals, Systems and Computers*, Nov. 2003, pp. 54–59.
- [14] D. Rabideau, "Ubiquitous MIMO digital array radar," in *Proc. 37th Asilomar Conf. Signals, Systems, and Computers*, Nov. 2003, pp. 1057–1064.
- [15] E. Fishler, A. Haimovich, R. Blum, L. Cimini, D. Chizhik, and R. Valenzuela, "MIMO radar: An idea whose time has come," in *Proc. 2004 IEEE Int. Conf. Radar*, Apr. 2004, pp. 71–78.
- [16] D.R. Fuhrmann and G. San Antonio, "Transmit beamforming for MIMO radar systems using partial signal correlation," in *Proc. 38th Asilomar Conf. Signals, Systems and Computers*, Nov. 2004, pp. 295–299.
- [17] F.C. Robey, S. Coultts, D. Weikle, J.C. McHarg, and K. Cuomo, "MIMO radar theory and experimental results," in *the 38th Asilomar Conference on Signals, Systems and Computers*, pp. 300–304, Nov. 2004.
- [18] I. Bekkerman and J. Tabrikian, "Target detection and localization using MIMO radars and sonars," *IEEE Trans. Signal Processing*, vol. 54, pp. 3873–3883, Oct. 2006.
- [19] L. Xu, J. Li, and P. Stoica, "Adaptive techniques for MIMO radar," *14th IEEE Workshop Sensor Array and Multi-channel Processing*, Waltham, MA, July 2006, pp. 258–262.
- [20] E. Fishler, A. Haimovich, R. Blum, L. Cimini, D. Chizhik, and R. Valenzuela, "Spatial diversity in radars—Models and detection performance," *IEEE Trans. Signal Processing*, vol. 54, pp. 823–838, Mar. 2006.
- [21] N. Lehmann, A.M. Haimovich, R.S. Blum, and L. Cimini, "MIMO-radar application to moving target detection in homogenous clutter," presented at Adaptive Sensor Array Processing Workshop at MIT Lincoln Laboratory, Waltham, MA, July 2006.
- [22] N.H. Lehmann, A.M. Haimovich, R.S. Blum, and L.J. Cimini, "High resolution capabilities of MIMO radar," in *Proc. 40th Asilomar Conf. Signals, Systems and Computers*, Nov. 2006, pp. 25–30.
- [23] G.J. Foschini, "Layered space-time architecture for wireless communication in a fading environment when using multiple antennas," *Bell Labs Tech. J.*, vol. 1, no. 2, pp. 41–59, 1996.
- [24] V. Tarokh, N. Seshadri, and A. Calderbank, "Space-time codes for high data rate wireless communication: Performance criterion and code construction," *IEEE Trans. Inform. Theory*, vol. 44, pp. 744–765, Mar. 1998.
- [25] E. Fishler, A. Haimovich, R. Blum, L. Cimini, D. Chizhik, and R. Valenzuela, "Performance of MIMO radar systems: advantages of angular diversity," in *Proc. 38th Asilomar Conf. Signals, Systems and Computers*, vol. 1, pp. 305–309, Nov. 2004.
- [26] M. Skolnik, *Introduction to Radar Systems*, 3rd ed. New York: McGraw-Hill, 2001.
- [27] Y. Yang and R.S. Blum, "Radar waveform design based on mutual information and mean-square error estimation," *IEEE Trans. Aerosp. Electron. Syst.*, vol. 43, no. 1, pp. 330–343, 2007.
- [28] I. Papoutsis, C.J. Baker, and H.D. Griffiths, "Fundamental performance limitations of radar networks," presented at Proc. 1st EMRS DTC Technical Conf., Edinburgh, 2004 [Online]. Available: [www.emrsdct.com/conferences/2004/downloads/pdf/tech\\_conf\\_papers/A07.pdf](http://www.emrsdct.com/conferences/2004/downloads/pdf/tech_conf_papers/A07.pdf)
- [29] R. Viswanathan and P.K. Varshney, "Distributed detection with multiple sensors I: Fundamentals," *Proc. IEEE*, vol. 85, pp. 54–63, Jan. 1997.
- [30] R.S. Blum, S.A. Kassam, and H.V. Poor, "Distributed detection with multiple sensors II: Advanced topics," *Proc. IEEE*, vol. 85, pp. 64–79, Jan. 1997.
- [31] R.S. Blum, "Distributed detection for diversity reception of fading signals in noise," *IEEE Trans. Inform. Theory*, vol. 48, pp. 158–164, Jan. 1999.
- [32] P.M. Woodward, *Probability and Information Theory with Application to Radar*. Norwood, MA: Artech House, 1953.
- [33] N. Lehmann, E. Fishler, A.M. Haimovich, R.S. Blum, D. Chizhik, L. Cimini, and R. Valenzuela, "Evaluation of transmit diversity in MIMO-radar direction finding," *IEEE Trans. Signal Processing*, vol. 55, no. 2, pp. 2215–2225, 2007.
- [34] N. Lehmann, *Some Contributions on MIMO Radar*, Ph.D. dissertation, New Jersey Institute of Technology, 2006.
- [35] B.D. Steinberg, "The peak sidelobe of the phased array having randomly located elements," *IEEE Trans. Antennas Propagat.*, vol. AP-20, pp. 129–136, Mar. 1972.
- [36] B.D. Steinberg and E.H. Attia, "Sidelobe reduction of random arrays by element position and frequency diversity," *IEEE Trans. Antennas Propagat.*, vol. AP-31, pp. 922–930, Nov. 1982.

